Hydathode immunity against the vascular pathogen *Xanthomonas campestris* pv. campestris by the Arabidopsis CNL-type receptor SUT1

Short title:

Hydathode immunity by Arabidopsis CNL-type receptor SUT1

Author list:

Nanne W. Taks[1], Marieke van Hulten[1], Jeroen A. van Splunter-Berg[1], Sayantani Chatterjee[1], Misha Paauw[1], Sebastian Pfeilmeier[1] and Harrold A. van den Burg[1]

Author affiliations:

1) Molecular Plant Pathology, Swammerdam Institute for Life Sciences, Faculty of Science, University of Amsterdam, Science Park 904, 1098 XH, Amsterdam, the Netherlands

***Author for correspondence:** H.A. van den Burg

Email: H.A.vandenBurg@uva.nl, Tel +31 20 525 7797

Figures: 4

Supporting figures: 7

Supporting data files: 4

Abstract

Bacterial plant pathogens exploit natural openings, such as pores or wounds, to enter the plant interior and cause disease. Plants actively guard these openings through defense mechanisms that have been described extensively for stomates, the most common points of entry. However, bacteria from the genus *Xanthomonas* have specialized in that they enter their host via hydathodes—a poorly studied organ at the leaf margin involved in guttation. While hydathodes can mount an effective immune response against bacteria, a dedicated perception mechanism still needs to be discovered. To identify a hydathode-specific immune receptor, we mapped a novel resistance gene against *X. campestris* pv. campestris (Xcc) in Arabidopsis using an inoculation procedure that promotes natural entry via hydathodes. Using Recombinant Inbred Lines (RILs) between susceptible accession Oy-0 and resistant Col-0, a QTL for resistance was identified on the right arm of Chromosome 5 in Col-0. Combining this finding with results of a genome-wide association analysis, a single candidate gene was fine-mapped that encoded a coiled-coil nucleotide-binding leucine-rich repeat (CNL) immune receptor protein called SUPPRESSOR OF TOPP4 1 (SUT1). Whereas the ZAR1 immune receptor acts in the vasculature against Xcc, we establish that SUT1 already restricts Xcc in hydathodes but is ineffective in the vasculature. In corroboration, we confirm promoter activity of *SUT1* in the epithem tissue within hydathodes. Altogether, we provide evidence for an NLR that confers hydathode-specific resistance in Arabidopsis against infection by Xcc.

Author summary

Black rot disease, caused by the bacterial pathogen *Xanthomonas campestris* pv. campestris (Xcc), is an economically relevant disease of cabbage crops. Xcc is rather unique in that it enters the plant interior through specialized organs at the edge of the leaf. These structures called hydathodes contain water pores and are involved in leaf water regulation. Although we know that hydathodes can mount an immune response against these bacteria, specific immune receptors still need to be discovered. In our search for hydathode resistance mechanisms, we use the model plant *Arabidopsis thaliana* to identify genetic targets that could be translated to cabbage breeding practices. Here, by screening large populations of genetically diverse Arabidopsis plants, we could pinpoint a genetic locus that is involved in hydathode resistance. On this locus, we identified a gene, *SUT1*, that confers resistance against Xcc, restricting early hydathode colonization by the bacteria and reducing subsequent disease symptoms. Interestingly, this resistance is ineffective in later stages of infection when the bacteria colonize the plant vascular system. Therefore, this study provides new insights in hydathode-specific resistance and opens doors for more research on these tissue- or organ-specific resistance mechanisms in plants.

Introduction

Plant pathogenic microbes exploit different strategies to invade their host and induce disease. Foliar bacterial pathogens primarily take advantage of natural openings of

84 plants, such as pores involved in gas exchange (stomata) or water and nutrient
85 homeostasis (hydathodes). Consequently, plants have evolved a plethora of immune
86 mechanisms to guard these openings, responding to the presence of pathogens [1,2].
87 Among these entry points, stomata are arguably the most widely studied in the context
88 of plant immunity. Several immune mechanisms have been elucidated over the past
89 years, including sensing of microbe-associated molecular patterns (MAMPs), such as
90 bacterial flagellin [3] or fungal chitin [4]. Upon perception, plants activate a signaling
91 cascade that includes pre-invasive closure of the stomatal pores followed by post-
92 invasive opening [5–7]. While stomata provide access to the leaf apoplast, hydathodes
93 represent an entry point for highly specialized bacterial pathogens that colonize the
94 leaf vasculature [8–10]. The hydathode anatomy is composed of an enclosed
95 extracellular cavity interspersed with specialized epithem cells. The cavity is
96 connected to the exterior via stomata-like openings in the epidermis called water pores
97 [11,12]. Water pores allow water exudation, called guttation, in conditions when root
98 pressure exceeds water evaporation [13]. The cavity is connected to endings of xylem
99 trachea and in part filled with the epithem tissue, which is hypothesized to act as an
100 active filter of the guttation fluid. Interestingly, the water pores do not completely close
101 in response to pathogens [8,14], providing nearly unrestricted access to the hydathode
102 cavity. Several pathogenic *Xanthomonas* spp. are known to invade their hosts via
103 hydathodes [8,9,15]. Despite the absence of pre-invasive immunity, a post-invasive
104 immune response is mounted in hydathodes against both hydathode-adapted and
105 non-adapted bacterial pathogens [16], which restricts bacterial proliferation in the
106 cavity and thereby reduces the number of vascular outbreaks. Intriguingly, although
107 general immune signaling hubs have been confirmed to be involved in this hydathode
108 immune response, the existence of hydathode-specific immune receptors still needs
109 to be demonstrated.

110 Plant immune receptors can be classified as cell-surface and intracellular receptors
111 [17,18]. While cell-surface pattern recognition receptors (PRRs) generally detect well-
112 conserved microbe-associated molecular patterns (MAMPs), intercellular nucleotide-
113 binding leucine-rich repeat (NLR) receptors respond directly or indirectly to the mode
114 of action of effector proteins. These effector promote virulence upon delivery to the
115 host cell to manipulate cellular processes including the suppression of plant immunity
116 [19]. The plant NLRs can be divided into three subgroups based on the N-terminal

117 domains: Coiled-coil (CC) NLRs (CNLs), Toll/Interleukin-1 receptor/Resistance (TIR)
118 NLRs (TNLs), and RPW8-like CC domain (RPW8) helper NLRs (RNLs). While some
119 NLRs can activate immune responses by themselves through oligomerization into a
120 so-called resistosome complex [20], others rely on helper NLRs or are part of an NLR
121 network to confer immune signaling [18]. The evolution of plant immune receptor
122 networks and pathogen immune suppressors has shaped the landscape of most plant-
123 pathogen interactions [17].

124 These immune receptors and pathogen effectors have been studied extensively in
125 *Arabidopsis thaliana* (hereafter Arabidopsis) for several bacterial pathogens, in
126 particular *Pseudomonas syringae* [21], a stomatal pathogen. For hydathode-infecting
127 bacteria, such as *Xanthomonas campestris* pv. campestris (Xcc) [10], only a few
128 resistance mechanisms, for instance NLR-mediated recognition of the Xcc effector
129 XopAC (AvrAC) by HOPZ-ACTIVATED RESISTANCE (ZAR1), have been unraveled
130 [22,23]. However, this latter finding was achieved using inoculation methods that
131 circumvent the natural infection path via hydathodes, thereby overlooking any
132 resistance mechanisms unique to hydathodes. Furthermore, many Arabidopsis
133 accessions, including Col-0, still display a considerable level of resistance against Xcc
134 strains that lack XopAC [16], indicating the presence of additional resistance
135 mechanisms.

136 Limited research has been conducted on pathogen recognition and defense
137 mechanisms within hydathodes. It is known for example that in cabbage, lignin is
138 deposited in and around the hydathodes in association with Xcc infections [24]. In
139 cauliflower, a necrotic response was detected around hydathodes in response to Xcc
140 [8], indicating some form of a hypersensitive response (HR) that is often associated
141 with plant immunity [25,26]. This response was found to be more pronounced when
142 using an Xcc mutant defective in the type three secretion system (T3SS). The T3SS
143 is responsible for translocating bacterial effector proteins into host cells, suggesting
144 that Xcc type three effectors (T3Es) are involved in immune suppression within
145 hydathodes. Furthermore, a strain in which the *xopAC* gene is deleted induces a
146 stronger necrotic response in cauliflower than the wildtype strain [8], corroborating the
147 idea that hydathodes themselves can already mount an effective immune response
148 upon pathogen recognition when the hydathode cavity is colonized by Xcc.

149 Additional data from Arabidopsis hydathodes supports this notion, as mutants lacking
150 PRR co-receptors BRI1-ASSOCIATED RECEPTOR KINASE 1 (BAK1) and its close
151 homolog BKK1 (BAK1-LIKE 1, SERK4) are more susceptible to hydathode
152 colonization by bacterial pathogens [16]. In addition, the immune signaling hub formed
153 by the proteins ENHANCED DISEASE SUSCEPTIBILITY 1 (EDS1) – PHYTOALEXIN
154 DEFICIENT 4 (PAD4) – ACTIVATED DISEASE RESISTANCE 1 (ADR1) was shown
155 to be involved in restricting hydathode colonization. On top of that, a formate
156 dehydrogenase (AtFDH1), known to be involved in several abiotic stresses, is linked
157 to restricting hydathodes from being colonized by Xcc [27]. Hence, it becomes
158 apparent that an effective, post-invasive immune response exists in plants against
159 bacteria in hydathodes, yet the causal receptors for this tissue-specific immune
160 recognition remain elusive to this date. To fill this knowledge gap on hydathode
161 immunity, we set out to identify the plant immune receptors in Arabidopsis that mount
162 an effective immune response against Xcc and study if this response is already
163 effective in hydathodes.

164 Results

165 A QTL on Chromosome 5 is associated with resistance against Xcc 166 *ΔxopAC*

167 In a recent study, we showed that the Arabidopsis accession Col-0 shows a high level
168 of resistance to the vascular bacterial pathogen Xcc8004 in natural (guttation-based)
169 infections and that this response was independent of the recognition of the effector
170 XopAC by the ZAR1 resistosome [16]. Furthermore, the study showed that the
171 accession Oy-0 is hypersusceptible to the same bacterial strain. To map the causal
172 gene(s) for this unknown resistance trait(s), we used an existing Arabidopsis
173 population of Recombinant Inbred Lines (RILs) between Oy-0 × Col-0 composed of
174 500 RILs [28]. In total, we screened 165 RILs of this population, including the two
175 parental lines Oy-0 and Col-0, for resistance using a bioluminescent reporter strain
176 (Tn*5*:*lux*) of Xcc8004 *ΔxopAC* [16,29]. For each plant, the three most-symptomatic
177 leaves were sampled at 14 days post inoculation (dpi) and bacterial colonization was
178 visualized using light-sensitive films (Fig 1A). The level of resistance was then scored
179 using a luminescence index ordinal scale [29] and normalized to the Oy-0 control for
180 each experiment (Figs 1B and C). Using an Expectation-maximization (EM) model for

181 a single QTL [30] and LOD threshold set at 2.49 by permutation (n = 1000), three QTLs
182 were identified, that is, one at Chromosome 4 and two on Chromosome 5 (Fig 1D).
183 These QTLs showed an explained variance (EV) of 10, 11 and 32%, respectively. The
184 QTL at the end of the right arm of Chromosome 5 had an LOD score of 14.92 and thus
185 displayed a strong genetic association with the resistance phenotype in the Oy-0 ×
186 Col-0 RIL population.

187 Genome-wide association study (GWAS) identified candidate R-
188 gene *SUT1*

189 To identify candidate genes in this strong QTL, a GWAS was performed with the same
190 Xcc8004 *ΔxopAC* Tn*5:lux* reporter strain on the Arabidopsis HapMap population,
191 consisting of 360 natural accessions [31]. Disease assays were performed on a subset
192 of 321 lines and disease was scored 14 dpi and normalized to Oy-0 control. GWA
193 analysis was performed on phenotypic data in an online GWA portal, using an imputed
194 SNP dataset of over five million SNPs [32]. Unexpectedly, no SNPs were identified
195 with a significant correlation to the disease phenotype on Chromosome 5. However,
196 several SNPs that were close to the False Discovery Rate (FDR) significance
197 thresholds coincided with the most significant QTL in the Oy-0 × Col-0 population (Fig
198 1E), indicating an association with disease. These SNPs were located in the coding
199 sequence of the gene At5g63020, which codes for SUPPRESSOR OF TOPP4
200 (SUT1), a previously characterized CNL involved in plant immunity [33]. Combining
201 the results of the RIL and the GWAS analyses, we concluded that the *SUT1* gene
202 could be involved in resistance against Xcc in Arabidopsis.

203 **Fig 1. Mapping of *SUT1* as a candidate R-gene against Xcc8004 *ΔxopAC* in**
204 **Arabidopsis Col-0. A)** Disease symptoms and bacterial luminescence in the resistant
205 Col-0 and hypersusceptible Oy-0 accessions following spray inoculation with
206 bioluminescent Xcc8004 *ΔxopAC.* Leaves shown are representative of spray
207 inoculation with either Tn*5:lux* or Tn*7:lux* tagged reporter strains. Bacterial spread is
208 visualized on light-sensitive film 14 days post inoculation (dpi). **B)** Histogram depicting
209 the variation in luminescence index score 14 dpi (normalized to Oy-0) for all 165 Oy-
210 0 × Col-0 Recombinant Inbred Lines (RILs) following spray inoculation with Xcc8004
211 *ΔxopAC* Tn*5:lux*. **C)** Population structure of 165 RILs in the Oy-0 × Col-0 RIL
212 population, ordered by luminescence index score at 14 dpi (normalized to Oy-0) shown

213 in B). **D)** QTL graph showing LOD scores for each of the 85 markers in the RIL
214 population (Expectation-maximization algorithm). LOD significance threshold
215 determined by permutation (n = 1000) at 2.49 **E)** Manhattan plot of Chromosome 5
216 from a screen of 321 accession present in the HapMap collection. Highlighted SNPs
217 in orange are located within the coding sequence of *SUT1*. False Discovery Rate
218 (FDR) thresholds set at $-\log_{10}$ (p) = 8 (Bonferroni) and $-\log_{10}$ (p) = 7.29 (Benjamini-
219 Hochberg).

220 SUT1 is involved in hydathode resistance against Xcc

221 To further investigate the role of SUT1 in the differential immune response between
222 Oy-0 and Col-0, we aligned the respective *SUT1* alleles and identified seven SNPs in
223 the $SUT1^{Oy\text{-}0}$ coding sequence, of which six are non-synonymous and were predicted
224 to result in amino acid substitutions (Figs 2A and S1). Five of these predicted
225 substitutions are in the leucine-rich repeat (LRR) domain, which is known to be a
226 surface for protein-protein interactions [34] and is often involved in target sensing
227 and/or ligand binding [20,35]. Notably, the stop codon in $SUT1^{Col\text{-}0}$ is replaced by an
228 Arginine codon in $SUT1^{Oy\text{-}0}$ (CGA), leading to a predicted 17-residue peptide extension
229 of $SUT1^{Oy\text{-}0}$, which potentially could reach into the binding pocket of the LRR domain
230 based on the Alphafold2 protein structure prediction (Figs 2A and S2-S3). These
231 sequence differences between $SUT1^{Col\text{-}0}$ and $SUT1^{Oy\text{-}0}$ could explain the difference in
232 disease resistance due to impairment of $SUT1^{Oy\text{-}0}$ to mount an immune response
233 against Xcc8004 *ΔxopAC*. To test if a null allele in Col-0 would lead to loss-of-
234 resistance, we assessed Xcc disease susceptibility in *sut1* T-DNA insertion mutants.
235 Two T-DNA insertion lines, *sut1-8* and *sut1-9* (Fig 2B), were previously shown to
236 display a loss of SUT1-mediated autoimmunity in a *topp4-1* background [33], implying
237 the absence of a functional *SUT1* gene. To confirm a role of SUT1 in Xcc resistance,
238 we performed spray inoculations assays with Xcc8004 *ΔxopAC* Tn*7:lux* and assessed
239 the level of resistance both in hydathodes (7 dpi) and late stages of infection (14 dpi).
240 Compared to the wildtype Col-0 control, both *sut1* T-DNA insertion lines showed an
241 increased number of hydathodes with severe bacterial infections at 7 dpi (Figs 2C and
242 D), more pronounced leaf chlorosis (Figs 2C and E) combined with a more advanced
243 bacterial spread across the infected leaves at 14 dpi (Figs 2C and F). During both the
244 early and late stages of infection, *sut1* knockouts showed an intermediate
245 susceptibility phenotype compared to plants of the immunocompromised *bak1-5;bkk1-*

246 *1* (*bb*) and the hypersusceptible Oy-0 accession. This corroborates the identification
247 of several QTLs with significant LOD scores in the RIL population (Fig 1D) indicative
248 for the presence of one or more loci involved in disease resistance, in addition to
249 *SUT1*. A previous study showed that SUT1 mediates an auto-immune response in a
250 genetic background that encodes a specific modification in a TYPE 1 PROTEIN
251 PHOPSHATASE 4 (TOPP4), suggesting that SUT1 guards the TOPP4 protein [33].
252 To infer if TOPP4 is also important for Xcc resistance in Col-0, a previously
253 characterized *topp4* knockout line was inoculated with Xcc8004 *ΔxopAC* Tn*7:lux*. A
254 small but significant increase in the number of heavily infected hydathodes was seen
255 in the *topp4* knockout line, but no increase in the bacterial spread across the leaf or
256 leaf chlorosis during later infection stages (Fig S4), suggesting that the SUT1-
257 mediated immunity to Xcc does not act through guarding TOPP4. These results
258 indicate that SUT1 restricts Xcc proliferation inside the hydathodes, thereby reducing
259 Black rot disease symptoms and the systemic colonization of the plant vasculature
260 during later infection stages.

261 **Fig 2. SUT1 contributes to early hydathode resistance against Xcc8004**
262 ***ΔxopAC.* A)** Predicted SUT1 protein model. Arrows depict predicted amino acid
263 substitutions in Oy-0 vs. Col-0. **B)** *SUT1* gene model depicting Col-0 allele and
264 approximate sites of the T-DNA insertions in the *sut1-8* and *sut1-9*. **C)** Spray
265 inoculation of *sut1-8* and *sut1-9* with Xcc8004 *ΔxopAC* Tn*7:lux.* Wildtype background
266 (Col-0), *bak1-5;bkk1-1* (Col-0) and the accession Oy-0 were included as controls.
267 *Top,* visualization of high density hydathode colonization using light sensitive films (7
268 dpi); *bottom*, visualization of the systemic spread of Xcc and disease symptom
269 development (14 dpi). **D,E,F)** Number of infected hydathodes 7 dpi (**D**), chlorotic
270 area 14 dpi (**E**) and bacterial colonization 14 dpi (**F**) per leaf for each line in C)
271 following spray inoculation with Xcc8004 *ΔxopAC* Tn*7:lux*. In panel D, the circle size
272 depicts the number (#) of leaves with a certain score (y-axis) from three independent
273 repetitions. Of note, the *sut1* mutants show an increased number of hydathode
274 infections 7 dpi, culminating in more pronounced disease symptoms and increased
275 bacterial spread compared to wildtype control 14 dpi (Col-0). Note that Oy-0 is still
276 more susceptible than the *sut1* mutants. Significance letters from non-parametric
277 Kruskal-Wallis test with Dunn's Post-Hoc test, p-value threshold = 0.05.

278 ## *SUT1* is active in hydathodes

279 As SUT1-mediated resistance occurs in hydathodes, we hypothesized that the *SUT1*
280 gene is expressed in the hydathode epithem cells. To investigate this, transgenic
281 reporter lines were generated to study the activity of the *SUT1* promoter by fusing a
282 2.1 kb DNA fragment upstream of the start codon to the *β-glucuronidase (GUS*)
283 reporter gene for histochemical analysis. We detected GUS straining throughout the
284 leaves of 4-week-old T1 transgenic plants (Figs 3A and S5), with strong saturation in
285 hydathode tissue, indicating expression patterns of *SUT1*. To determine whether this
286 GUS staining corresponds to true expression in the epithem tissue, we used a second
287 independent reporter system, *NLS-3×mVENUS* [36]. As reference for epithem cells,
288 we used the epithem marker line *pPUP1::RCl2A-tdTomato* [16], which shows red
289 fluorescence at the epithem cell membrane (Fig 3B). Col-0 plants carrying the
290 *pSUT1::NLS-3×mVENUS* constructs showed fluorescent mVENUS signal in the nuclei
291 of epithem cells and throughout the mesophyll tissue (Figs 3C and S6). Taken
292 together, our data confirm the expression of *SUT1* in the hydathodes.

293 **Fig 3. *SUT1* is expressed in epithem cells within hydathodes. A)** Arabidopsis
294 *pSUT1::GUS* lines stained with X-gluc show expression of *SUT1* throughout 4-week-
295 old leaves. Strong saturation of signal can be seen in hydathode tissue (white
296 arrows). **B)** Arabidopsis epithem marker line *pPUP1::RCl2a-tdTomato* shows
297 tdTomato localization in epithem cell membrane within hydathodes. Epithem cells
298 can be distinguished from mesophyll cells in the bright-field image (white dashed
299 line). **C)** Arabidopsis *pSUT1::NLS3×mVENUS* T_2 line shows accumulation of
300 mVENUS in nuclei of mesophyll and epithem cells. Epithem cells can be
301 distinguished from mesophyll cells in the bright-field image (white dashed line).
302 Images were taken of epidermal peels and are representative of three independent
303 lines (Fig S6).

304 SUT1-mediated resistance is ineffective when hydathodes are 305 bypassed

306 As SUT1 provides resistance to Xcc already during the early stages of infection, we
307 assessed whether SUT1 also contributes to resistance at later stages of the infection
308 or upon wound infection when the bacteria cause a systemic infection along the leaf
309 vasculature. To this end, clipping inoculations were used to provide the bacteria with
310 direct access to the midvein and some lateral veins near the leaf apex, thereby

311 bypassing the hydathodes. We quantified both the bacterial spread along the midvein
312 and the relative chlorotic leaf area (as a proxy of disease symptom development) (Fig
313 4A). Strikingly, the analysis revealed that the SUT1-mediated resistance was lost
314 when the hydathodes were bypassed as shown by similar levels of leaf chlorosis in
315 the different genetic backgrounds (Fig 4B). Moreover, by quantifying the total distance
316 the bacteria had progressed along the midvein, we found that long distance movement
317 and colonization itself appears to be unchanged in *sut1-9* compared to the Col-0
318 wildtype control (Fig 4C). This implies that SUT1 does not provide a high level of
319 resistance to Xcc when the bacteria are directly introduced into vascular tissue by leaf
320 clipping. This tissue-specific response is different from ZAR1-mediated resistance,
321 which remains effective even when the bacteria are introduced directly into the midvein
322 (Fig S7). Overall, we report here on the identification of an NLR that contributes to
323 resistance against Xcc primarily in hydathodes.

324 **Fig 4. SUT1 resistance against Xcc is ineffective when hydathodes are**
325 **bypassed during inoculation. A)** Disease symptoms and bacterial spread in Col-0
326 leaves at 7 dpi following clip inoculation with Xcc8004 *ΔxopAC* Tn*7:lux*. Bacterial
327 progression is quantified as the spread of the luminescence signal along the
328 midvein. **B,C)** Chlorotic leaf area (**B**) and bacterial spread along the midvein (**C**) 7
329 dpi following clip inoculation with Xcc8004 *ΔxopAC* Tn*7:lux*. SUT1 resistance against
330 Xcc is apparently ineffective in the vasculature of Col-0 when the hydathodes are
331 bypassed and the bacteria are introduced using leaf clipping. Significance letters
332 from a two-way ANOVA with Tukey Post-Hoc test, p-value threshold = 0.05.

333 Discussion

334 Here, we characterized a role for Arabidopsis SUT1 as a functional immune receptor
335 in natural infections by Xcc. We show that SUT1 acts primarily in hydathodes,
336 restricting Xcc colonization in early stages of infection and thereby reducing the
337 subsequent systemic spread of Xcc and with that the onset of disease symptoms.
338 Interestingly, SUT1-mediated resistance is strongly compromised when the
339 hydathodes are bypassed, indicating that SUT1 confers a first layer of defense in the
340 Xcc disease cycle. This role of SUT1 in hydathodes differs from other reports on Xcc
341 immunity in Arabidopsis, such as the ZAR1 immune response mounted upon
342 recognition of XopAC activity [23] and the AMAR1-mediated hypersensitive response

343 through interaction with the T3E XopAM [37]. In addition, the SUT1-mediated
344 resistance mechanism seems to be independent of MAPK signaling cascades, as
345 knockout lines of several MAPK phosphatases (MKPs) show increased vascular
346 spread and symptom development when Xcc is directly introduced into the vasculature
347 [22], while under our conditions *sut1* knockout lines do not. Therefore, the role of SUT1
348 in plant defense in specialized cells in hydathodes is thus far unique compared to that
349 of characterized NLRs in Arabidopsis [17,38]. In corroboration, *SUT1* gene is
350 expressed in the epithem cells within hydathodes.

351 As *SUT1* encodes an intercellular immune receptor, our data support the notion that
352 Xcc actively manipulates epithem tissue to gain access to the vascular system of the
353 plant. Importantly, the causal agent for activation of SUT1-mediated immunity remains
354 unknown albeit that an indirect activation mechanism of SUT1 through guarding the
355 TOPP4 phosphatase has been proposed in the context of auto-immunity [33]. While
356 we did not find evidence for this TOPP4 guard-guardee model in the interaction with
357 Xcc (Fig S4), the two closest homologs of SUT1 in Arabidopsis, RESISTANT TO P.
358 SYRINGAE 5 (RPS5) and SUPPRESSOR OF MKK1 MKK2 2 (SUMM2) [33], have
359 both been described as 'guards' in plant-pathogen interactions [39,40], which
360 highlights the possibility of a similar function of SUT1. TOPP4 is part of an Arabidopsis
361 gene family of highly similar protein phosphatases called TOPP1 to TOPP9. This
362 family is involved in abscisic acid (ABA) signaling and leaf water homeostasis [41,42].
363 Interestingly, multiple TOPP family members are targeted by the *Pseudomonas*
364 *syringae* T3E AvrE during infection to hijack ABA signaling thereby suppressing the
365 reopening of the stomata upon bacterial entry to induce water soaking of the leaf
366 apoplast—a phenomenon that supports bacterial colonization of the leaf apoplast [43–
367 45]. Interestingly, Xcc8004 is known to employ T3E XopAM, which belongs to the
368 same protein superfamily of conserved bacterial effectors as *Pseudomonas* AvrE [46].
369 Nonetheless, AvrE superfamily members can exhibit a wide variety of functions [47]
370 and recent work using Y2H-screens on an Arabidopsis cDNA library did not reveal a
371 protein-protein interaction between XopAM and individual TOPPs [37]. Although the
372 elicitor of SUT1-mediated resistance has not been identified, it might be associated
373 with manipulation of TOPPs and therefore ABA signaling.

374 How manipulation of ABA signaling might benefit a hydathode pathogen remains
375 unclear. While *Pseudomonas syringae* actively manipulates the stomatal aperture by

376 targeting ABA signaling [44,45], hydathode pores are known to not fully close in
377 response to (a)biotic stresses [8]. Indirect evidence for bacterial manipulation of ABA
378 signaling in hydathodes comes from the observation that *Pseudomonas* naturally does
379 not progress towards the leaf vascular tissue yet it can colonize and proliferate in
380 hydathodes [16]. Besides *Pseudomonas*, members of the *Xanthomonas* genus are
381 also known to affect ABA levels during infection. For example, transcription activator-
382 like effector (TALE) Tal8 from *Xanthomonas translucens* pv. undulosa (Xtu), the
383 causal agent of bacterial leaf streak, induces the expression of a host gene encoding
384 9-*cis*-epoxycarotenoid dioxygenase (*TaNCED-5BS*), which catalyzes a rate-limiting
385 step in ABA biosynthesis [48]. Although Xcc8004 does not harbor TALEs [49], some
386 evidence exists for the manipulation of ABA synthesis in Arabidopsis through induction
387 of the Arabidopsis homolog of *NCED5* by the T3E XopAH (AvrXccC) and increased
388 virulence of Xcc when ABA is applied exogenously [50]. Moreover, ABSCISIC ACID-
389 RESPONSIVE 1 (ABR1), a negative regulator of ABA, is required for resistance
390 against *Xanthomonas campestris* pv. vesicatoria (Xcv) in pepper [51]. Altogether,
391 these findings underline the importance of ABA signaling as a target for bacterial
392 manipulation including many members of the *Xanthomonas* genus, but how ABA plays
393 a role in Xcc hydathode colonization remains elusive.

394 When it comes to hydathode colonization, we see an intermediate level of resistance
395 in the *sut1* knockout lines in the Col-0 background compared to the hypersusceptible
396 accession Oy-0. This indicates the presence of other resistance mechanisms against
397 Xcc in hydathodes. Indeed, we observed two additional QTLs on Chromosome 4,
398 which were not fine mapped in this study. The underlying genes for these QTLs might
399 encode additional NLRs, receptor-like proteins (RLPs) or receptor-like kinases (RLKs),
400 some of which are known to be specifically expressed in hydathodes [52]. It seems
401 that the resistance phenotype seen in Col-0, in absence of ZAR1-mediated resistance,
402 can still be based on several and possibly disconnected resistance mechanisms of
403 which SUT1 resistance appears to be a major contributor. The existence of a wide
404 array of immune receptors in Arabidopsis holds promise for application of these genes
405 in *Brassica* crops to ensure durable resistance. As was shown in other crop-pathogen
406 interactions, *R*-gene stacking is less readily overcome by pathogens than the
407 implementation of single *R*-genes [53–55].

408 In summary, we identified a CNL-type immune receptor, SUT1, that acts in hydathodes
409 where it reduces Xcc virulence by limiting the initial hydathode colonization and
410 thereby the subsequent disease development due to vascular spread of the bacteria.
411 This hydathode-specific response is different from other known plant immune
412 responses against vascular pathogens, as the efficacy of the *SUT1* gene is lost when
413 this initial barrier of the hydathode is bypassed using clip inoculations that mimic
414 wound damage. How the SUT1-mediated immune response is activated in epithem
415 tissue will be part of future studies, although SUT1 likely acts as a guard of one or
416 more TOPPs or other plant phosphatases. Studying host manipulation by Xcc is a
417 promising model to elucidate the intricate interactions that are happening in
418 hydathodes in response to bacterial pathogens.

419 Materials and Methods

420 Plant growth conditions

421 *Arabidopsis thaliana* lines used are listed in S1 Table. For all experiments, seeds were
422 stratified for three to four days on wet filter paper at 4 °C in the dark, and then sown in
423 40-pot trays (Desh Plantpak, Tray Danish size 40 cell (8x5)) in slitpots (Pöppelmann
424 Teku, S 5,5 LB), using potting soil (Jongkind Substrates, Hol80 zaaigrond Nr 1) to
425 which 500 ml Entonem suspension (Koppert Biological Systems, approximately 1.6 x
426 10^6 third stage *Steinernema feltiae* nematode larvae) was added per tray to prevent
427 black fly multiplication in growth chambers. Hereafter, trays were placed in standard
428 short day (SD) conditions (11/13h light/dark, 22 °C, RH 70%). For the first five days
429 after sowing, trays were covered with transparent plastic domes to ensure seedling
430 growth.

431 Plasmid and transgenic plant generation

432 Primer sequences and plasmids used are listed in S1 Table. The plasmids to create
433 the *pSUT1::GUS* and *pSUT1::NLS-3×mVENUS* reporter lines in Arabidopsis were
434 assembled using the GreenGate system [56]. First, a 2.1 kb fragment upstream of the
435 start codon of *SUT1* (*AT5G63020*) in Col-0 was synthesized with external *Bsa*I sites
436 (Eurofins Genomics). Next, the *NLS-3×mVENUS* module was amplified from
437 pGreenII-229-NLS-3×mVENUS [36] with added *Bsa*I sites and cloned into pGGA000.
438 Final binary vectors were then assembled in the backbone pGGZ003 with either *GUS*

439 or *NLS-3×mVENUS* as CDS module using a multisite Goldengate reaction, leading to
440 pGGZ_pSUT1_GUS_tUBQ10_BastaR and pGGZ_SUT1_NLS-
441 3×mVENUS_tUBQ10_BastaR. These plasmids were electroporated into
442 *Agrobacterium tumefaciens* strain GV3101 carrying pSOUP and Arabidopsis Col-0
443 was transformed using the floral dip method [57]. Several independent transgenic lines
444 were analyzed for each construct.

445 *Xanthomonas* disease assays

446 Spray inoculations with bioluminescent Xcc *ΔxopAC* (Tn*5:lux* or Tn*7:lux*) were
447 performed according to previous studies [29,16]. Briefly, Xcc strains were plated on
448 KADO medium [58] with the appropriate antibiotics and grown for 48-72 hours at 28
449 °C. Bacteria were collected, washed once with 10 mM $MgSO_4$ and diluted to OD_{600} =
450 0.1. Silwet L-77 was added to a final concentration of 0.0002% and bacteria were
451 sprayed on 4-to-5-week-old Arabidopsis plants (Preval sprayer, SKU# 0221).
452 Inoculated plants were subjected to two guttation cycles over two days in a climate
453 incubator (Snijders Labs, MC1000) to promote hydathode infection. In these cycles,
454 temperature and relative humidity are raised (25°C, RH 95%) to induce guttation, after
455 which a rapid drop in temperature and humidity (21°C, RH 70%) leads to re-uptake of
456 guttation droplets. Subsequently, plants are placed for an additional 12 days at SD
457 growth conditions (11/13h light/dark, 24-22 °C, RH 70%) in the same incubator.
458 Clipping assays were performed by cutting 5 mm of the apex of each leaf (three leaves
459 per plant) with scissors dipped in bacterial inoculum (OD_{600} = 0.1). Plants were
460 subjected to the same two-day guttation cycle and placed for an additional five days
461 at SD growth conditions in an MC1000 climate chamber.

462 Detection of luminescent bacteria

463 For spray inoculations, the three most diseased leaves of each plant were sampled 7
464 dpi and 14 dpi. Each leaf was glued onto an A3 white paper sheet using a grid and
465 covered with a transparent plastic sheet [29]. Next, a light-sensitive X-ray film (Fuji
466 Super RX) was placed on top and left for exposure overnight. The film was developed
467 the next morning and scanned, alongside the leaves, using an A3 flatbed scanner
468 (Epson Expression 12000XL). For 7 dpi, the obtained images were overlayed in Adobe
469 Photoshop 2023/2024 to count the number of luminescent hydathodes per leaf. At 14
470 dpi, scans of leaves and light-sensitive film were analyzed using the ScAnalyzer image

471 analysis script [59] to determine chlorosis and bacterial colonization. For clipping
472 assays, at 7 dpi, leaves were sampled in the same manner. For analysis, chlorosis
473 and bacterial colonization were analyzed with ScAnalyzer. Bacterial progression
474 through the midvein was measured using Fiji (ImageJ).

475 RIL screen and QTL analysis

476 The Oy-0 × Col-0 RIL population [28] was received from the INRA Versailles stock
477 center (). From the 470 RILs in the population, 165 (including the parental Oy-0 and
478 Col-0) were selected for disease assays (S2 Table). For analysis, the mean
479 luminescence index score [29] per leaf (n = 18) for each line was normalized to the
480 score of Oy-0 and used as input for QTL mapping in R using the R/qtl package version
481 1.66 [30]. LOD scores for each of the 85 markers were determined in a single QTL
482 model using the Expectation-maximization (EM) algorithm. LOD thresholds were
483 determined by permutation (n = 1000). Explained variance (EV) per QTL was
484 calculated as $EV(\%) = (1 - 10(-2 * LOD/n) * 100$, where LOD is the LOD score and
485 n is the number of RILs.

486 GWA screen and analysis

487 The HapMap seed collection was received from NASC (Borevitz lab; NASC ID,
488 N76309; ABRC ID, CS76309). From the 360 lines in the population, 321 accessions
489 (including the controls Oy-0 and Col-0) were selected for disease assays (S3 Table).
490 The mean luminescence index score [29] per leaf (n = 18) for each line was normalized
491 to Oy-0. As input for GWA analysis, the data was transformed in a binary score in
492 which 0 = <50% and 1 = >50% of Oy-0. These phenotypes were analyzed in the GWA
493 portal [32] using the Imputed Fullsequence Dataset, TAIR 9, containing over five
494 million SNPs [60]. P-values were obtained by applying an accelerated mixed model
495 (AMM) [61]. False Discovery Rate (FDR) thresholds were set at $-\log_{10}(p) = 8$
496 (Bonferroni) and $-\log_{10}(p) = 7.29$ (Benjamini-Hochberg). SNPs with $-\log_{10}(p)$ values >
497 6 are documented in S3 Table.

498 GUS staining and imaging

499 Transgenic GUS lines were grown for 4-5 weeks at standard SD conditions. Rosettes
500 were taken from soil, washed in double distilled water and submerged in GUS staining
501 solution (0.5 mM $K_3Fe(CN)_6$, 0.5 mM $K_4Fe(CN)_6$, 0.1 M $NaPO_4$ (pH 7.0), 10 mM EDTA,

502 0.1% (v/v) Triton X-100 and 1 mg/ml X-Gluc in double distilled water) [62] in a 50 ml
503 falcon tube. Rosettes were twice vacuum infiltrated for two minutes and then incubated
504 at 37 °C for two hours to avoid overstaining [62]. To destain, rosettes were incubated
505 in 96% ethanol at room temperature for two days. The destaining solution was
506 replaced twice until all chlorophyll had been removed. Leaves were imaged using a
507 stereomicroscope (Leica MZ FLIII + Nikon Digital Sight DS-Fi2).

508 Imaging fluorescent reporter lines

509 Fluorescent reporter lines were grown for 4-5 weeks using SD conditions (13D/11L).
510 To enable imaging of exposed hydathode tissue, fully expanded leaves were picked
511 and stripped of the epidermal cell layer [63] using household sellotape. Leaves were
512 then imaged with a digital inverted fluorescence microscope (ThermoFisher EVOS fl,
513 RFP filter for tdTomato, YFP filter for mVENUS).

514 Protein sequence alignments

515 Coding sequences from both the Arabidopsis alleles of *SUT1* in Col-0 and Oy-0 were
516 downloaded from Araport11 (Tair10)[64] and translated *in silico*. Predicted protein
517 sequences were then aligned in R with ClustalOmega using the Biostrings (v.2.68.1)
518 and msa (v.1.32.0) packages.

519 Alphafold2 protein structure predictions

520 Alphafold2 [65] predictions were performed using ColabFold (v.1.5.5) and MMseqs2
521 using default settings [66]. Out of the five given models, the model with the highest
522 rank score was used for visualization of the predicted fold. Alphafold2 .pdb files are
523 available in S1 and S2 File.

524 Quantification and statistical analyses

525 All data analyses and plotting were done in R (v.4.3.2). For statistical analysis of
526 parametric data, a two-way ANOVA followed by a Tukey post-hoc test was performed
527 to detect differences between groups. For non-parametric data, such as hydathode
528 counts or proportional data, a Kruskal-Wallis test followed by a Dunn's post-hoc test
529 was performed. All experiments were performed in at least three independent
530 repetitions with similar results. Data from repetitions was pooled for visualization and
531 statistical analysis.

Acknowledgements

We would like to thank Ludek Tikovsky and Harold Lemereis for the excellent care of our plants in the greenhouse. We also want to thank Manon Richard for previous work on fluorescent reporter lines in Arabidopsis. Lastly, we want to thank Niko Geldner, Laurent Noël and Gail Preston for sharing materials. This research was supported by the Topsector T&U TKI programs “Stop natural entry” and “Finding the Achilles’ heel of Brassica for Black Rot disease” (grants EZ-2012-02 and TU18024 to H.A.v.d.B.) and the breeding companies Bejo Zaden B.V. and Rijk Zwaan.

Competing interests

Authors declare no competing interests.

Supporting information

S1 Fig. Alignment of predicted SUT1 protein sequences of the Arabidopsis accessions Col-0 and Oy-0. Coding sequences of *SUT1*$^{Col\text{-}0}$ and *SUT1*$^{Oy\text{-}0}$ were obtained from Araport11 and translated *in silico* into amino acid sequences. Alignment depicts six predicted amino acid substitutions in SUT1$^{Oy\text{-}0}$ compared to SUT1$^{Col\text{-}0}$, of which one is predicted to result in a 17-residue peptide extension at the C-terminus in SUT1$^{Oy\text{-}0}$.

(TIFF)

S2 Fig. Alphafold2 predictions of SUT1$^{Col\text{-}0}$ and SUT1$^{Oy\text{-}0}$. Alphafold2 fold prediction for the rank 1 model of SUT1$^{Col\text{-}0}$ (**A**) SUT1$^{Oy\text{-}0}$ (**B**), colored by pLDDT score from high (blue) to low (red). pLDDT score for best 5 models is shown in right panel. N- and C-termini show low pLDDT scores, indicating low predictive value.

(TIFF)

560 **S3 Fig. Alphafold2 predictions indicate that SUT1^{Oy-0} C-terminal extension**
561 **might interfere with its protein function. A)** Alphafold2 fold prediction of SUT1^{Col-0},
562 colored by functional domains (CC, NBS-ARC & LRR). **B)** Alphafold2 fold prediction
563 of SUT1^{Oy-0}, colored by functional domains (CC, NBS-ARC & LRR). Green residues
564 indicate differences at amino acid level compared to SUT1^{Col-0}. C-terminal peptide in
565 SUT1^{Oy-0} is predicted in the LRR pocket. **C)** Superimposed model of SUT1^{Col-0} and
566 SUT1^{Oy-0}. Green residues indicate differences at amino acid level in SUT1^{Oy-0}.

567 (TIFF)

568 **S4 Fig. SUT1-mediated resistance in Arabidopsis Col-0 does not depend on**
569 **TOPP4 function. A)** Number of infected hydathodes per leaf at 7 dpi following spray
570 inoculation with Xcc8004 *ΔxopAC* Tn*7:lux*. Circles depict number of leaves for each
571 score. The topp4 knockout line shows a slight increase in hydathode infections
572 compared to the Col-0 control. Significance letters from non-parametric Kruskal-
573 Wallis test with Dunn's Post-Hoc test, p-value threshold = 0.05. **B)** Bacterial
574 colonization defined as percentage of total leaf area colonized per leaf following
575 spray inoculation with Xcc8004 *ΔxopAC* Tn*7:lux* (14 dpi). Bacterial colonization was
576 calculated using ScAnalyzer [59]. The *topp4* knockout line does not display
577 increased bacterial spread compared to the wildtype control (Col-0). Significance
578 letters from non-parametric Kruskal-Wallis test with Dunn's Post-Hoc test, p-value
579 threshold = 0.05.

580 (TIFF)

581 **S5 Fig. *SUT1* is expressed in hydathodes and mesophyll.** Two independent
582 homozygous T3 lines of 4-week-old Arabidopsis *pSUT1::GUS* show GUS enzymatic
583 activity in hydathodes (black arrows) and mesophyll tissue throughout the leaf.
584 Leaves were incubated in GUS staining solution for two hours.

585 (TIFF)

586 **S6 Fig. *SUT1* is expressed in epithem cells within hydathodes.** Three
587 independent T2 lines of 4-week-old Arabidopsis *pSUT1::NLS-3×mVENUS* show
588 accumulation of mVENUS in nuclei of mesophyll and epithem cells. Epithem cells
589 can be distinguished from mesophyll cells in the bright-field image (white dashed
590 line).

591 (TIFF)

592 **S7 Fig. ZAR1-mediated immunity is effective in the leaf vasculature. A)** Disease
593 symptoms and bacterial luminescence in resistant Col-0 and susceptible *zar1-1*
594 knockout lines, 7 dpi following clip inoculation with Xcc8004 WT Tn*5:lux*. **B,C)**
595 Chlorotic leaf area (**B**) and bacterial spread along the midvein (**C**) 7 dpi following clip
596 inoculation with Xcc8004 WT Tn*5:lux* on Arabidopsis Col-0, *bak1-5;bkk1-1*, *zar1-1*,
597 *rks1-1* and Oy-0. ZAR1-mediated resistance against Xcc is effective in the
598 vasculature of Col-0 and *bak1-5;bkk1-1* when the hydathodes are bypassed and the
599 bacteria are introduced using leaf clipping. Significance letters from a two-way
600 ANOVA with Tukey Post-Hoc test, p-value threshold = 0.05.

601 (TIFF)

602 **S1 Table. List of strains, genotypes and oligonucleotides used in this study.**

603 (XLSX)

604 **S2 Table. Raw data of RIL population genetic structure and disease scoring.**

605 (XLSX)

606 **S3 Table. Raw data on disease scoring of HapMap population for GWAS.**

607 (XLSX)

608 **S1 File. SUT1 Col-0 Alphafold2 fold prediction model 1**

609 (PDB)

610 **S2 File. SUT1 Oy-0 Alphafold2 fold prediction model 1**

611 (PDB)

612 # References

613 1. Melotto M, Zhang L, Oblessuc PR, He SY. Stomatal defense a decade later.
614 Plant Physiol. 2017;174(2):561–71.

615 2. Zhang J, Coaker G, Zhou JM, Dong X. Plant immune mechanisms: from
616 reductionistic to holistic points of view. Mol Plant. 2020;13(10):1358–78.

617 3. Zipfel C, Robatzek S, Navarro L, Oakeley EJ, Jones JDG, Felix G, et al. Bacterial
618 disease resistance in Arabidopsis through flagellin perception. Nature. 2004 Apr
619 1;428(6984):764–7.

620 4. Miya A, Albert P, Shinya T, Desaki Y, Ichimura K, Shirasu K, et al. CERK1, a
621 LysM receptor kinase, is essential for chitin elicitor signaling in Arabidopsis.
622 Proc Natl Acad Sci. 2007;104(49):19613–8.

623 5. Liu Z, Hou S, Rodrigues O, Wang P, Luo D, Munemasa S, et al. Phytocytokine
624 signalling reopens stomata in plant immunity and water loss. Nature. 2022 May
625 12;605(7909):332–9.

626 6. Melotto M, Underwood W, Koczan J, Nomura K, He SY. Plant stomata function in
627 innate immunity against bacterial invasion. Cell. 2006;126(5):969–80.

628 7. Thor K, Jiang S, Michard E, George J, Scherzer S, Huang S, et al. The calcium-
629 permeable channel OSCA1. 3 regulates plant stomatal immunity. Nature.
630 2020;585(7826):569–73.

631 8. Cerutti A, Jauneau A, Auriac MC, Lauber E, Martinez Y, Chiarenza S, et al.
632 Immunity at Cauliflower Hydathodes Controls Systemic Infection by
633 *Xanthomonas campestris* pv *campestris*. Plant Physiol. 2017 Jun;174(2):700–
634 16.

635 9. Gluck-Thaler E, Cerutti A, Perez-Quintero AL, Butchacas J, Roman-Reyna V,
636 Madhavan VN, et al. Repeated gain and loss of a single gene modulates the
637 evolution of vascular plant pathogen lifestyles. Sci Adv. 2020 Nov
638 13;6(46):eabc4516.

639 10. Hugouvieux V, Barber CE, Daniels MJ. Entry of *Xanthomonas campestris* pv.
640 *campestris* into Hydathodes of *Arabidopsis thaliana* Leaves: A System for
641 Studying Early Infection Events in Bacterial Pathogenesis. Mol Plant-Microbe
642 Interactions®. 1998 Jun;11(6):537–43.

643 11. Cerutti A, Jauneau A, Laufs P, Leonhardt N, Schattat MH, Berthomé R, et al.
644 Mangroves in the leaves: anatomy, physiology, and immunity of epithemal
645 hydathodes. Annu Rev Phytopathol. 2019;57:91–116.

646 12. Jauneau A, Cerutti A, Auriac MC, Noël LD. Anatomy of leaf apical hydathodes in
647 four monocotyledon plants of economic and academic relevance. PLoS One.
648 2020;15(9):e0232566.

649 13. Routaboul JM, Bellenot C, Clément G, Citerne S, Remblière C, Charvin M, et al.
650 Arabidopsis hydathodes are sites of intense auxin metabolism and nutrient
651 scavenging. bioRxiv; 2022.

652 14. Bellenot C, Routaboul JM, Laufs P, Noël LD. Hydathodes. Curr Biol.
653 2022;32(14):R763–4.

654 15. Jian Y, Gong D, Wang Z, Liu L, He J, Han X, et al. How plants manage
655 pathogen infection. EMBO Rep. 2024;25(1):31–44.

656 16. Paauw M, van Hulten M, Chatterjee S, Berg JA, Taks NW, Giesbers M, et al.
657 Hydathode immunity protects the Arabidopsis leaf vasculature against
658 colonization by bacterial pathogens. Curr Biol. 2023 Feb;S0960982223000131.

659 17. Ngou BPM, Ding P, Jones JDG. Thirty years of resistance: Zig-zag through the
660 plant immune system. Plant Cell. 2022 May 1;34(5):1447–78.

661 18. Ngou BPM, Jones JDG, Ding P. Plant immune networks. Trends Plant Sci. 2022
662 Mar;27(3):255–73.

663 19. Büttner D. Behind the lines–actions of bacterial type III effector proteins in plant
664 cells. FEMS Microbiol Rev. 2016;40(6):894–937.

665 20. Wang J, Hu M, Wang J, Qi J, Han Z, Wang G, et al. Reconstitution and
666 structure of a plant NLR resistosome conferring immunity. Science.
667 2019;364(6435):eaav5870.

668 21. Xin XF, Kvitko B, He SY. Pseudomonas syringae: what it takes to be a
669 pathogen. Nat Rev Microbiol. 2018 May;16(5):316–28.

670 22. Lin H, Wang M, Chen Y, Nomura K, Hui S, Gui J, et al. An MKP-MAPK protein
671 phosphorylation cascade controls vascular immunity in plants. Sci Adv.
672 2022;8(10):eabg8723.

673 23. Wang G, Roux B, Feng F, Guy E, Li L, Li N, et al. The decoy substrate of a
674 pathogen effector and a pseudokinase specify pathogen-induced modified-self
675 recognition and immunity in plants. Cell Host Microbe. 2015;18(3):285–95.

676 24. Gay PA, Tuzun S. Involvement of a novel peroxidase isozyme and lignification
677 in hydathodes in resistance to black rot disease in cabbage. Can J Bot. 2000
678 Sep 1;78(9):1144–9.

679 25. Lam E, Kato N, Lawton M. Programmed cell death, mitochondria and the plant
680 hypersensitive response. Nature. 2001 Jun 1;411(6839):848–53.

681 26. Morel JB, Dangl JL. The hypersensitive response and the induction of cell death
682 in plants. Cell Death Differ. 1997 Dec 1;4(8):671–83.

683 27. Marzorati F, Vigani G, Morandini P, Murgia I. Formate dehydrogenase
684 contributes to the early Arabidopsis thaliana responses against Xanthomonas
685 campestris pv campestris infection. Physiol Mol Plant Pathol. 2021
686 Apr;114:101633.

687 28. Simon M, Loudet O, Durand S, Bérard A, Brunel D, Sennesal FX, et al. QTL
688 mapping in five new large RIL populations of Arabidopsis thaliana genotyped
689 with consensus SNP markers. Genetics. 2008;178(2253):64.

690 29. van Hulten M, Chatterjee S, van den Burg HA. Infection Assay for Xanthomonas
691 campestris pv. campestris in Arabidopsis thaliana Mimicking Natural Entry via
692 Hydathodes. In: Plant Innate Immunity. Humana, New York, NY: Springer;
693 2019. p. 159–85.

694 30. Broman KW, Wu H, Sen Ś, Churchill GA. R/qtl: QTL mapping in experimental
695 crosses. bioinformatics. 2003;19(7):889–90.

696 31. Weigel D, Mott R. The 1001 genomes project for Arabidopsis thaliana. Genome
697 Biol. 2009;10:1–5.

698 32. Seren Ü. GWA-Portal: Genome-Wide Association Studies Made Easy. In:
699 Ristova D, Barbez E, editors. Root Development: Methods and Protocols
700 [Internet]. New York, NY: Springer New York; 2018. p. 303–19. Available from:
701 https://doi.org/10.1007/978-1-4939-7747-5_22

702 33. Yan J, Liu Y, Huang X, Li L, Hu Z, Zhang J, et al. An unreported NB-LRR
703 protein SUT1 is required for the autoimmune response mediated by type one
704 protein phosphatase 4 mutation (topp4-1) in Arabidopsis. Plant J.
705 2019;100(2):357–73.

706 34. Padmanabhan M, Cournoyer P, Dinesh-Kumar SP. The leucine-rich repeat
707 domain in plant innate immunity: a wealth of possibilities. Cell Microbiol.
708 2009;11(2):191–8.

709 35. Martin R, Qi T, Zhang H, Liu F, King M, Toth C, et al. Structure of the activated
710 ROQ1 resistosome directly recognizing the pathogen effector XopQ. Science.
711 2020;370(6521):eabd9993.

712 36. Zhou F, Emonet A, Dénervaud Tendon V, Marhavy P, Wu D, Lahaye T, et al.
713 Co-incidence of Damage and Microbial Patterns Controls Localized Immune
714 Responses in Roots. Cell. 2020 Feb;180(3):440-453.e18.

715 37. Xie Q, Wei B, Zhan Z, He Q, Wu K, Chen Y, et al. Arabidopsis membrane
716 protein AMAR1 interaction with type III effector XopAM triggers a hypersensitive
717 response. Plant Physiol. 2023 Dec 1;193(4):2768–87.

718 38. Van de Weyer AL, Monteiro F, Furzer OJ, Nishimura MT, Cevik V, Witek K, et
719 al. A species-wide inventory of NLR genes and alleles in Arabidopsis thaliana.
720 Cell. 2019;178(5):1260-1272. e14.

721 39. Pottinger SE, Innes RW. RPS5-mediated disease resistance: fundamental
722 insights and translational applications. Annu Rev Phytopathol. 2020;58:139–60.

723 40. Zhang Z, Wu Y, Gao M, Zhang J, Kong Q, Liu Y, et al. Disruption of PAMP-
724 induced MAP kinase cascade by a Pseudomonas syringae effector activates
725 plant immunity mediated by the NB-LRR protein SUMM2. Cell Host Microbe.
726 2012;11(3):253–63.

727 41. Hou YJ, Zhu Y, Wang P, Zhao Y, Xie S, Batelli G, et al. Type one protein
728 phosphatase 1 and its regulatory protein inhibitor 2 negatively regulate ABA
729 signaling. PLoS Genet. 2016;12(3):e1005835.

730 42. Zhang J, Qin Q, Nan X, Guo Z, Liu Y, Jadoon S, et al. Role of protein
731 phosphatase1 regulatory subunit3 in mediating the abscisic acid response.
732 Plant Physiol. 2020;184(3):1317–32.

733 43. Hu Y, Ding Y, Cai B, Qin X, Wu J, Yuan M, et al. Bacterial effectors manipulate
734 plant abscisic acid signaling for creation of an aqueous apoplast. Cell Host
735 Microbe. 2022;30(4):518-529. e6.

736 44. Roussin-Léveillée C, Lajeunesse G, St-Amand M, Veerapen VP, Silva-Martins
737 G, Nomura K, et al. Evolutionarily conserved bacterial effectors hijack abscisic
738 acid signaling to induce an aqueous environment in the apoplast. Cell Host
739 Microbe. 2022 Apr;30(4):489-501.e4.

740 45. Xin XF, Nomura K, Aung K, Velásquez AC, Yao J, Boutrot F, et al. Bacteria
741 establish an aqueous living space in plants crucial for virulence. Nature. 2016
742 Nov;539(7630):524–9.

743 46. Degrave A, Siamer S, Boureau T, Barny MA. The AvrE superfamily: ancestral
744 type III effectors involved in suppression of pathogen-associated molecular
745 pattern-triggered immunity: The AvrE superfamily of type III effectors. Mol Plant
746 Pathol. 2015 Oct;16(8):899–905.

747 47. Nomura K, Andreazza F, Cheng J, Dong K, Zhou P, He SY. Bacterial pathogens
748 deliver water-and solute-permeable channels to plant cells. Nature.
749 2023;621(7979):586–91.

750 48. Peng Z, Hu Y, Zhang J, Huguet-Tapia JC, Block AK, Park S, et al.
751 Xanthomonas translucens commandeers the host rate-limiting step in ABA
752 biosynthesis for disease susceptibility. Proc Natl Acad Sci. 2019 Oct
753 15;116(42):20938–46.

754 49. Denancé N, Szurek B, Doyle EL, Lauber E, Fontaine-Bodin L, Carrère S, et al.
755 Two ancestral genes shaped the Xanthomonas campestris TAL effector gene
756 repertoire. New Phytol. 2018;219(1):391–407.

757 50. Ho YP, Tan CM, Li MY, Lin H, Deng WL, Yang JY. The AvrB_AvrC domain of
758 AvrXccC of Xanthomonas campestris pv. campestris is required to elicit plant
759 defense responses and manipulate ABA homeostasis. Mol Plant Microbe
760 Interact. 2013;26(4):419–30.

761 51. Choi DS, Hwang BK. Proteomics and functional analyses of pepper abscisic
762 acid–responsive 1 (ABR1), which is involved in cell death and defense
763 signaling. Plant Cell. 2011;23(2):823–42.

764 52. Wu Y, Xun Q, Guo Y, Zhang J, Cheng K, Shi T, et al. Genome-wide expression
765 pattern analyses of the Arabidopsis leucine-rich repeat receptor-like kinases.
766 Mol Plant. 2016;9(2):289–300.

767 53. Shehryar K, Khan RS, Iqbal A, Hussain SA, Imdad S, Bibi A, et al. Transgene
768 stacking as effective tool for enhanced disease resistance in plants. Mol
769 Biotechnol. 2020;62:1–7.

770 54. Zhang J, Hewitt TC, Boshoff WH, Dundas I, Upadhyaya N, Li J, et al. A
771 recombined Sr26 and Sr61 disease resistance gene stack in wheat encodes
772 unrelated NLR genes. Nat Commun. 2021;12(1):3378.

773 55. Zhu S, Li Y, Vossen JH, Visser RG, Jacobsen E. Functional stacking of three
774 resistance genes against Phytophthora infestans in potato. Transgenic Res.
775 2012;21:89–99.

776 56. Lampropoulos A, Sutikovic Z, Wenzl C, Maegele I, Lohmann JU, Forner J.
777 GreenGate-a novel, versatile, and efficient cloning system for plant
778 transgenesis. PloS One. 2013;8(12):e83043.

779 57. Clough SJ, Bent AF. Floral dip: a simplified method for Agrobacterium-mediated
780 transformation of Arabidopsis thaliana. Plant J. 1998;16(6):735–43.

781 58. Kado CI, Heskett MG. Selective media for isolation of agrobacterium,
782 Corynebacterium, Erwinia, Pseudomonas and Xanthomonas. Phytopathology.
783 1970;60(6):969–76.

784 59. Paauw M, Hardeman G, Taks NW, Lambalk L, Berg JA, Pfeilmeier S, et al.
785 ScAnalyzer: an image processing tool to monitor plant disease symptoms and
786 pathogen spread in Arabidopsis thaliana leaves. Plant Methods. 2024 May
787 31;20(1):80.

788 60. Atwell S, Huang YS, Vilhjálmsson BJ, Willems G, Horton M, Li Y, et al.
789 Genome-wide association study of 107 phenotypes in Arabidopsis thaliana
790 inbred lines. Nature. 2010;465(7298):627–31.

791 61. Zhang Z, Ersoz E, Lai CQ, Todhunter RJ, Tiwari HK, Gore MA, et al. Mixed
792 linear model approach adapted for genome-wide association studies. Nat
793 Genet. 2010;42(4):355–60.

794 62. Asai S, Cevik V, Jones JD, Shirasu K. Cell-specific RNA profiling reveals host
795 genes expressed in Arabidopsis cells haustoriated by downy mildew. Plant
796 Physiol. 2023;193(1):259–70.

797 63. Wu FH, Shen SC, Lee LY, Lee SH, Chan MT, Lin CS. Tape-Arabidopsis
798 Sandwich - a simpler Arabidopsis protoplast isolation method. Plant Methods.
799 2009 Nov 24;5(1):16.

800 64. Cheng CY, Krishnakumar V, Chan AP, Thibaud-Nissen F, Schobel S, Town CD.
801 Araport11: a complete reannotation of the Arabidopsis thaliana reference
802 genome. Plant J. 2017 Feb 1;89(4):789–804.

803 65. Jumper J, Evans R, Pritzel A, Green T, Figurnov M, Ronneberger O, et al.
804 Highly accurate protein structure prediction with AlphaFold. Nature. 2021 Aug
805 1;596(7873):583–9.

806 66. Mirdita M, Schütze K, Moriwaki Y, Heo L, Ovchinnikov S, Steinegger M.
807 ColabFold: making protein folding accessible to all. Nat Methods. 2022 Jun
808 1;19(6):679–82.

809

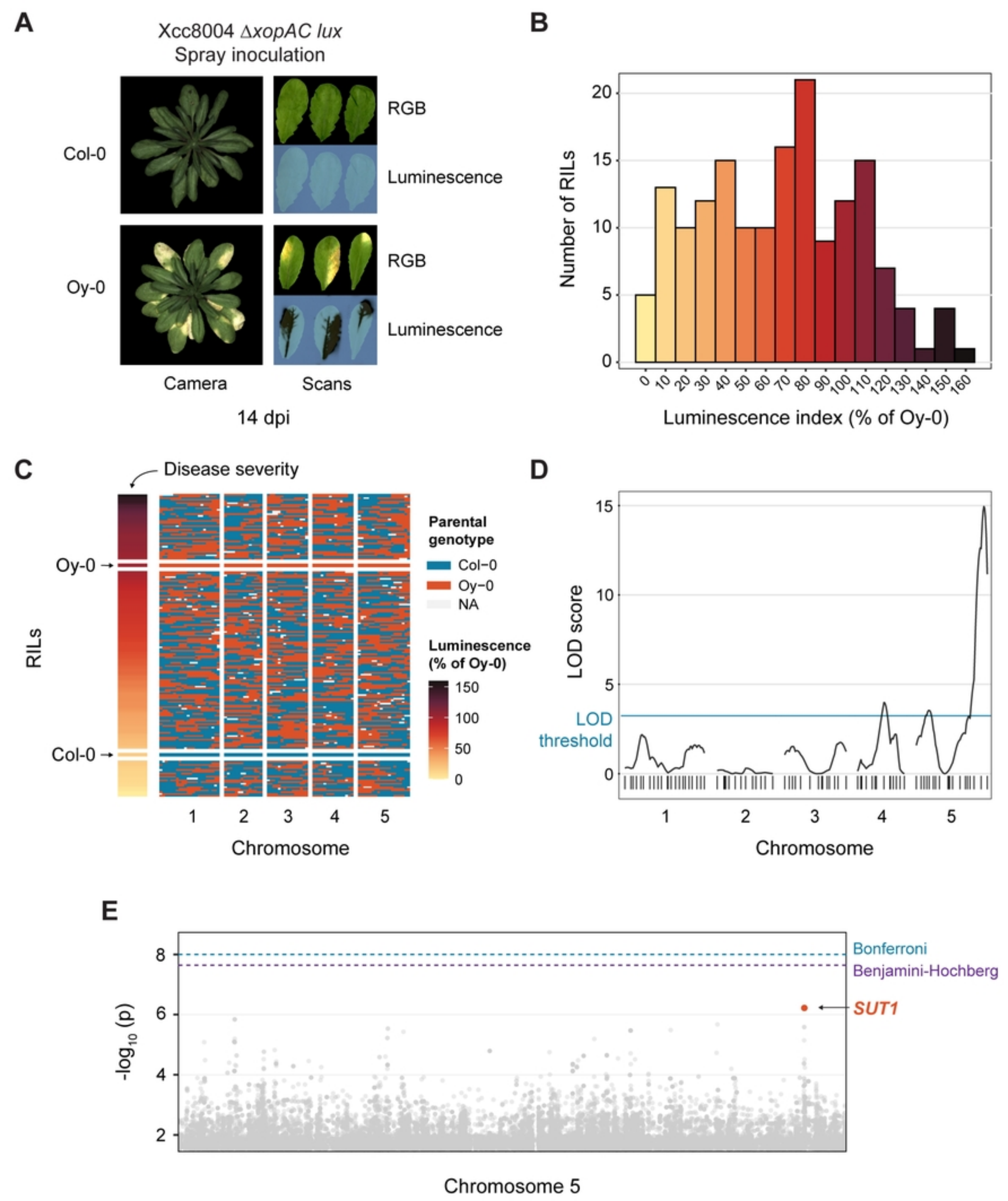
A
Xcc8004 ΔxopAC lux
Spray inoculation
Col-0
Oy-0
RGB
Luminescence
RGB
Luminescence
Camera
Scans
14 dpi
B
Number of RILs
Luminescence index (% of Oy-0)
C
Disease severity
Oy-0
Col-0
RILs
Parental genotype
Col−0
Oy−0
NA
Luminescence (% of Oy-0)
Chromosome
D
LOD score
LOD threshold
Chromosome
E
Bonferroni
Benjamini-Hochberg
SUT1
Chromosome 5

Fig 1

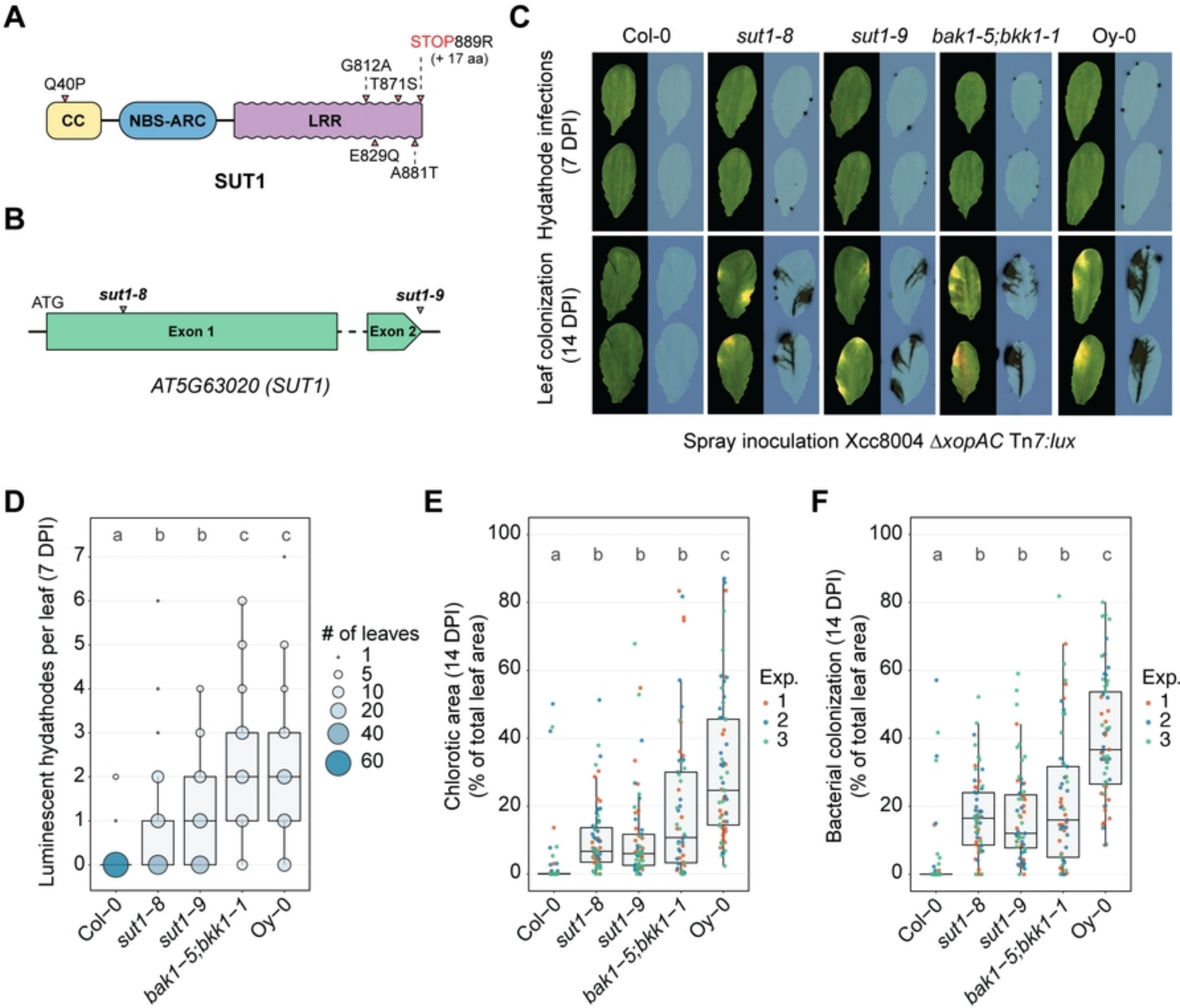
A
STOP889R
(+ 17 aa)
G812A
T871S
Q40P
CC
NBS-ARC
LRR
E829Q
A881T
SUT1
B
ATG
sut1-8
sut1-9
Exon 1
Exon 2
AT5G63020 (SUT1)
C
Col-0
sut1-8
sut1-9
bak1-5;bkk1-1
Oy-0
Hydathode infections (7 DPI)
Leaf colonization (14 DPI)
Spray inoculation Xcc8004 ΔxopAC Tn7:lux
D
Luminescent hydathodes per leaf (7 DPI)
# of leaves
1
5
10
20
40
60
Col-0
sut1-8
sut1-9
bak1-5;bkk1-1
Oy-0
E
Chlorotic area (14 DPI) (% of total leaf area)
Exp.
1
2
3
F
Bacterial colonization (14 DPI) (% of total leaf area)

Fig 2

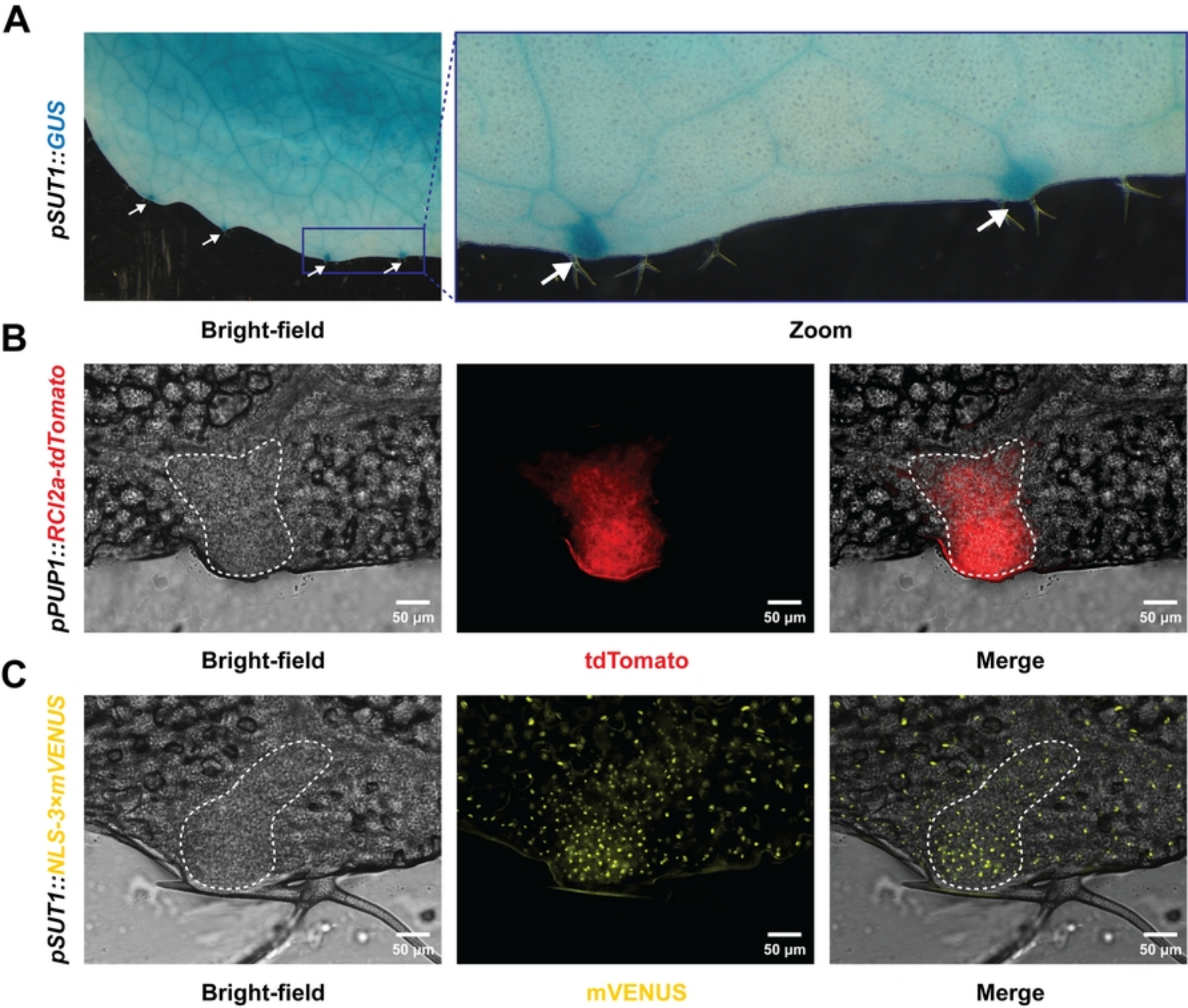
A
pSUT1::GUS
Bright-field
Zoom
B
pPUP1::RCI2a-tdTomato
50 µm
Bright-field
tdTomato
Merge
C
pSUT1::NLS-3×mVENUS
Bright-field
mVENUS
Merge

Fig 3

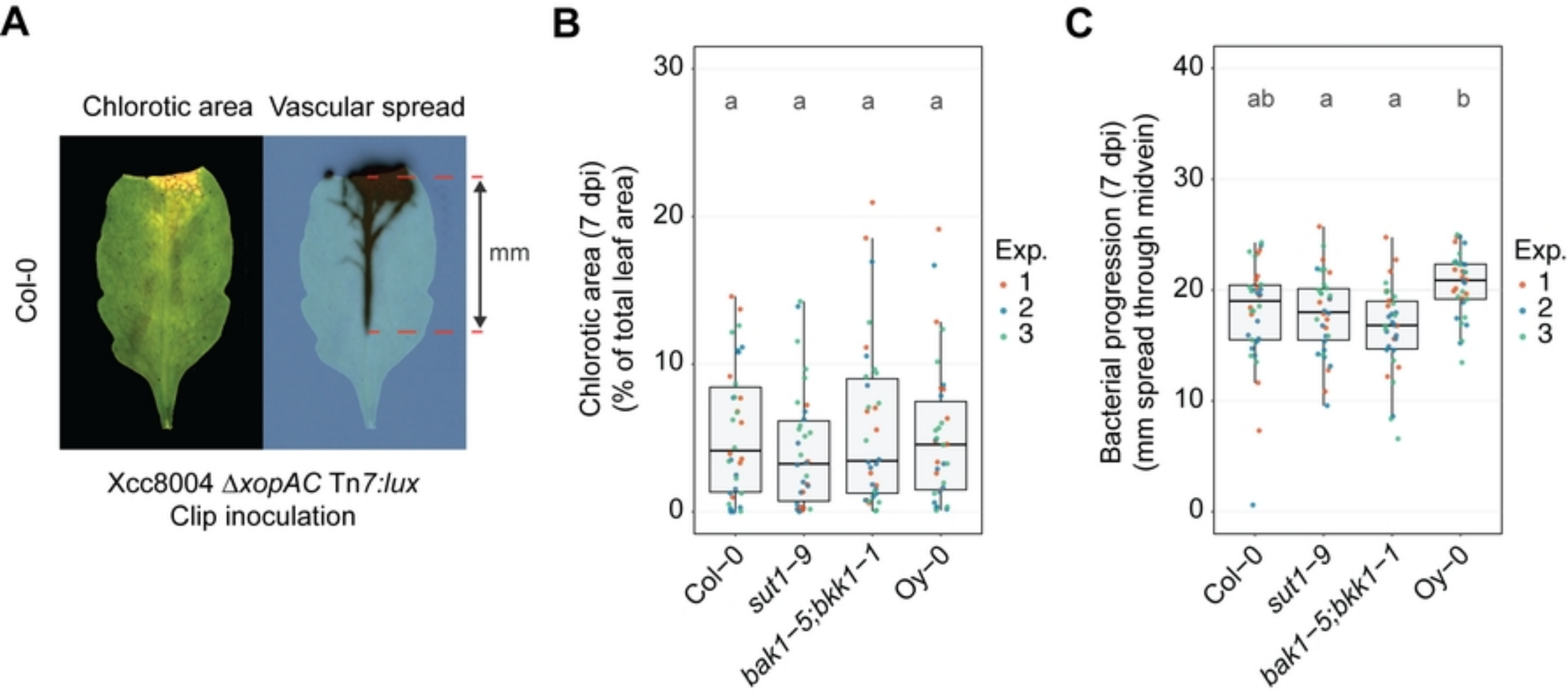
A
Chlorotic area
Vascular spread
Col-0
mm
Xcc8004 ΔxopAC Tn7:lux
Clip inoculation
B
Chlorotic area (7 dpi)
(% of total leaf area)
30
20
10
0
a
a
a
a
Col–0
sut1–9
bak1–5;bkk1–1
Oy–0
Exp.
1
2
3
C
Bacterial progression (7 dpi)
(mm spread through midvein)
40
30
20
10
0
ab
a
a
b
Col–0
sut1–9
bak1–5;bkk1–1
Oy–0
Exp.
1
2
3

Fig 4